

# Nanoscale Metrology of Line Patterns on Semiconductor by Continuous Wave Terahertz Multispectral Reconstructive 3-D Imaging Overcoming the Abbe Diffraction Limit

Anis Rahman<sup>1b</sup> and Aunik K. Rahman

**Abstract**—This paper demonstrates overcoming of the Abbe diffraction limit (ADL) on image resolution. Here, terahertz multispectral reconstructive imaging has been described and used for analyzing nanometer size metal lines fabricated on a silicon wafer. It has also been demonstrated that while overcoming the ADL is a required condition, it is not sufficient to achieve sub-nanometer image resolution with longer wavelengths. A nanoscanning technology has been developed that exploits the modified Beer-Lambert’s law for creating a measured reflectance data matrix and utilizes the “inverse distance to power equation” algorithm for achieving 3-D, sub-nanometer image resolution. The nano-lines images reported herein, were compared to scanning electron microscope (SEM) images. The terahertz images of 70 nm lines agreed well with the transmission electron microscope images. The 14 nm lines by SEM were determined to be ~15 nm. Thus, the wavelength dependent Abbe diffraction limit on image resolution has been overcome. Layer-by-layer analysis has been demonstrated where 3-D images are analyzed on any of the three orthogonal planes. Images of grains on the metal lines have also been analyzed. Unlike electron microscopes, where the samples must be in the vacuum chamber and must be thin enough for electron beam transparency, terahertz imaging is non-destructive, non-contact technique without laborious sample preparation.

**Index Terms**—Metrology, imaging, volume measurement, nanotechnology, nondestructive testing.

## I. INTRODUCTION

NANOMETER metal lines are the key for on chip interconnects where the feature sizes are approaching 10 nm and below. While fabrication of metal lines with 10 nm dimensions have been demonstrated, there is no obvious way for accurately measure their dimensions non-invasively. Current characterization techniques, such as scanning electron microscope (SEM), transmission electron microscope (TEM), atomic force microscope (AFM), scanning tunneling microscope (STM), and focused ion beam (FIB) have been established and practiced over the past decades. While these techniques are effective and accurate, they

are destructive, require tedious and time-consuming sample preparation. Additionally, the above-mentioned techniques produce a frozen-in-time image of a single surface. A semiconductor wafer, for example, must be cut for inspection across its thickness. Samples may be only as big as it may fit in the sample chamber that must be kept under high vacuum. Up until now, there has not been an alternative to characterizing a whole wafer, both on its surface and across the thickness, or the sub-surface, in a non-destructive, non-contact mode, with layer by layer inspection capability. Inevitably, semiconductor manufacturing is a complicated process where a wafer must undergo a number of critical tests, both in the blank form, at various stages of process development, and at the final stage with patterned devices. It is a laborious but unavoidable task to conduct testing at multiple stages for successful chip manufacturing. Especially, when the feature sizes are being reduced to 10 nm and below, the cost for multi-stage testing increases exponentially, which can significantly impact the cost of advanced technology products. Thus, the cost benefit to the end users that is expected from miniaturization of several orders of magnitude, is far from realization.

To this end, it appears that the scientific and the technical community is being held hostage to the fact that physics dictates that the ultimate image resolution is set by the wavelength of the light used for imaging, the Abbe diffraction limit (“ADL”). Ernst Abbe in 1873 [1] found that light with wavelength  $\lambda$ , traveling in a medium with refractive index  $n$  and converging to a spot with half-angle  $\theta$  will make a spot with radius,  $d = \frac{\lambda}{2n \sin \theta}$ , where,  $n \sin \theta$  is called the numerical aperture (NA). Approximating  $NA = 1$  (i.e., for vacuum), the lowest spot size (resolution) is  $\lambda/2$ . Since the wavelength of electrons is much smaller than that of photons (2.5 pm at 200 keV), the resolution of an electron microscope is theoretically unlimited. Practically, the resolution of an electron microscope is limited to ~0.1 nm due to its objective lens system.

Beating the diffraction limit has become one of the primary goal of research in modern optics [2], so, a question arises, “is the Abbe diffraction limit unavoidable?” The objective of the present work is to demonstrate one approach where the image formation mechanism is independent of the wavelength of the radiation used and thus, the Abbe diffraction limit has been avoided. We have recently reported on

Manuscript received April 25, 2018; revised June 21, 2018; accepted July 18, 2018. This paper is based in parts on a presentation made at the ASMC 2017, Saratoga Springs, NY. (Corresponding author: Anis Rahman.)

The authors are with Applied Research and Photonics, Inc., Harrisburg, PA 17111 USA (e-mail: a.rahman@arohotonics.net).

Color versions of one or more of the figures in this paper are available online at <http://ieeexplore.ieee.org>.

Digital Object Identifier 10.1109/TSM.2018.2865167

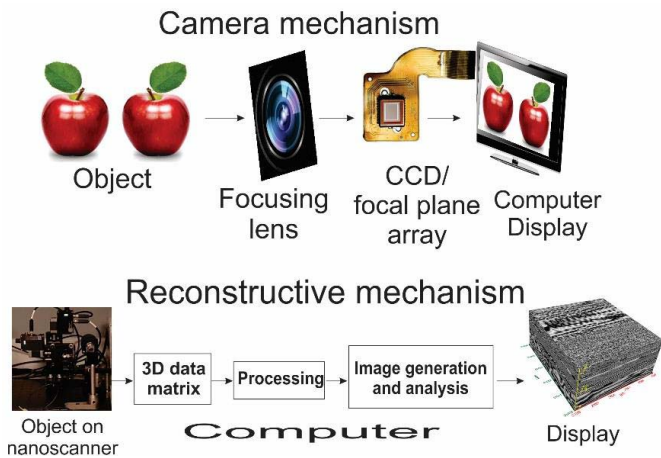


Fig. 1. Comparison of image formation scheme in a camera and in reconstructive imaging.

object that is focused on a CCD by means of a lens. The output  
of the CCD is processed by a built-in processor which displays  
the image and saves it in a file. In contrast, the reconstructive  
route eliminates the focusing lens and the CCD. Instead, the  
object to be imaged is scanned along the 3 orthogonal axes;  
the reflected signal (or, equivalently, the transmitted signal)  
is recorded in a data file and then processed by a suitable  
algorithm. The procedure for 3D image formation is outlined  
below; first the data structure and then the image formation  
algorithm are described followed by the required conditions  
for sub-nanometer image resolution.

#### A. Data Structure

3D imaging requires a value of a voxel, which is the small-  
est unit corresponding to a 3D space; i.e.,  $\{x, y, z, v\}$ , where  
 $\{x, y, z\}$  are the three orthogonal coordinates and  $v$  is the value  
of the reflected intensity at that point. To characterize a 3D  
space, data need to be recorded for all of a given 3D volume.  
This is best done by an experimental scanning protocol where  
the volume is divided into a number of slices (surfaces) and  
the slices are scanned one after another. Thus, the data are  
generated in the following sequence: for every  $\{z_1, y_1\}$ , a line  
is scanned giving  $\{x_1, x_2 \dots x_n\}$ . Then the line is repeated for  
 $y_2$  through  $y_n$ , while keeping the  $z_1$  (i.e., the depth) fixed.

This sequence of line scans at a given interval thus generates  
data for the first slice (surface) of the volume. Then, the whole  
scan is repeated for  $z_2$ , yielding the second slice of the vol-  
ume. This process is then repeated for all the slices along the  
Z-axis in order to digitize the whole volume. The line scan is  
done by a streaming data acquisition protocol, where, a com-  
mand is issued to move the scanner from the start point to the  
end point along the x-axis. As the positioning stage moves, its  
instantaneous position and the reflected intensity at that point  
are recorded by the computer interface; thus, generating the  
 $\{x_1, x_2 \dots x_n\}$  points for a given  $\{z_i, y_j\}$ . The reflected intensity,  
or both the reflected and transmitted intensity, is read simul-  
taneously corresponding to each  $x_i$ . Once the whole volume  
is scanned, the data set is then used for generating the image  
via a suitable algorithm such as the “inverse distance to power  
equations,” [6], [7] as described below.

#### B. Inverse Distance to Power Equation

This is a method for grid-based map creation from measured  
 $\{x, y, z, v\}$  data set. Practical  $\{x, y, z\}$  based data are typically  
comprised of irregularly spaced values; as such it requires fur-  
ther computation to generate a grid-based map (or a lattice).  
The gridding process effectively interpolates data values for  
the lattice at locations where data values are absent. Therefore,  
the closer the measured data points are to each other, the  
more accurate the gridded image is for feature sizes that  
are smaller than the hardware resolution. The experimental  
setup used for the present work has a hardware resolution  
of  $\sim 24$  nm. Therefore, the interpolation via inverse gridding  
method is used to generate an image at 1 nm resolution or  
less. The reliability of the interpolation is tested by calibration  
with respect to known dimensions [3]. A smoothing param-  
eter may be applied during interpolation in order to suit the

81 the multispectral reconstructive imaging of quantum dots [3],  
82 epitaxial semiconductor layers [4] as well as on soft tissues [5]  
83 where the dimension of the imaged objects are smaller than  
84 the wavelength of terahertz radiation (T-ray). The nanometer  
85 and sub-nanometer image resolution obtained by reconstruc-  
86 tive technique was validated by corresponding TEM images  
87 (except for the soft tissues where TEM images were not  
88 available); they were found in good agreement within the  
89 experimental error limits. As we will demonstrate below for  
90 the case of metal lines on silicon wafer, the technique reported  
91 herein does produce results in good agreement with SEM  
92 images as well. Therefore, it may be claimed that the tera-  
93 hertz multispectral reconstructive imaging technique reported  
94 in this paper is indeed capable of breaking the wavelength bar-  
95 rier as imposed by the Abbe diffraction limit. However, as will  
96 also be shown below, while overcoming the ADL is a required  
97 condition for achieving higher image resolution, it is not suf-  
98 ficient for achieving sub-nanometer image resolution. Hence,  
99 a stratagem has also been devised for achieving sub-nanometer  
100 image resolution.

101 In what follows, we first review the principle of reconstruc-  
102 tive imaging (RI) adapted in this work. Then we describe  
103 a stratagem for overcoming the ADL and achieving sub-  
104 nanometer image resolution. Afterwards, we present and ana-  
105 lyze images of nanometer size metal lines and compare them  
106 with corresponding SEM images followed by some concluding  
107 remarks.

## 108 II. MULTISPECTRAL RECONSTRUCTIVE IMAGING

109 Terahertz multispectral reconstructive imaging and tera-  
110 hertz time-domain spectrometry for investigating different  
111 semiconductor wafers and nanomaterials has been described  
112 elsewhere [3], [4]. Reconstructive imaging offers an important  
113 opportunity to define one’s own pixel size (or voxel size in 3D)  
114 by a hardware and software combination, as opposed to being  
115 limited by the image sensor chip such as the charged coupled  
116 device (CCD). A comparison of the mechanisms of a digital  
117 camera and the RI is shown in Fig. 1. As outlined (Fig. 1),  
118 a digital camera displays and records the processed signal of an

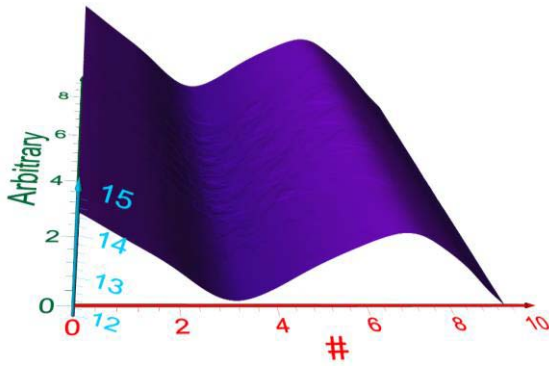


Fig. 2. A 3D plot of the function  $f(x, y, z) = c * \cos(x)$ .

174 imaging requirements for a given specimen. The method does  
 175 not extrapolate values beyond those found in the scanned  
 176 data matrix. The following equations are used for computation  
 177 of the 3D lattice via inverse distance to a power [7], [8]:

$$\hat{C}_j = \frac{\sum_{i=1}^n \frac{C_i}{h_{ij}^\beta}}{\sum_{i=1}^n \frac{1}{h_{ij}^\beta}} \quad (1)$$

179 where,  $h_{ij} = \sqrt{d_{ij}^2 + \delta^2}$ ,

180  $h_{ij}$  is the effective separation distance between grid node  
 181 “j” and the neighboring point “i;”

182  $\hat{C}_j$  are the interpolated values for lattice node “j;”

183  $C_i$  are the neighboring measured points;

184  $d_{ij}$  is the distance between grid node “j” and the neigh-  
 185 boring point “i;”

186  $\beta$  is the power or weighting parameter; and

187  $\delta$  is the smoothing parameter.

188 The power,  $\beta$  and the smoothing factor,  $\delta$ , in the above  
 189 computation may be chosen by the user to suit different imag-  
 190 ing needs. Once the lattice is calculated, the surface image  
 191 and volume image are generated by simply rendering the  
 192 grid with a chosen color scheme. As an illustration of the  
 193 functionality of the algorithm, consider a simple function,  
 194  $f(x, y, z) = c * \cos(x)$  to demonstrate the image formation.  
 195 One can easily compute this function over a given 3D space.  
 196 Let us assume the data range:  $x \rightarrow 0 \dots 3\pi$ ,  $y \rightarrow 0 \dots 6$ ,  $z$   
 197 and the value are calculated for a given  $c$ . Once the function  
 198 is evaluated via the procedure described above, one can con-  
 199 struct the data space. Then using the gridding method, one  
 200 can reconstruct (map) the function over the given 3D space.  
 201 The plot for the above function looks like as shown in Fig. 2.  
 202 Closer the grid points, smoother will be the surface. One can  
 203 plot experimental data by the same procedure.

### 204 C. Overcoming the Abbe Diffraction Limit and Achieving 205 Sub-Nanometer Resolution

206 As outlined in Fig. 1, the case of image formation by a cam-  
 207 era is totally dependent on the wavelength of the light used  
 208 for imaging; as such it must obey the Abbe diffraction limit.  
 209 Overcoming the ADL implies that the technique must be capa-  
 210 ble of resolving an object whose size is smaller than half the  
 211 wavelength of the energizing radiation.

In case of multispectral terahertz radiation (T-ray), the  
 wavelengths are much bigger than the visible spectrum. For  
 example, the terahertz source of the current experimental setup  
 has a range of 0.1 THz to  $\sim 33$  THz [9]. Thus, the wave-  
 length range is wide (multispectral); from  $\sim 9 \mu\text{m}$  up to  
 $\sim 3000 \mu\text{m}$ . Consequently, breaking the ADL demands that  
 one only needs to demonstrate a resolution of less than  $4.5 \mu\text{m}$   
 or so. Therefore, just overcoming the ADL in and of itself  
 is not sufficient to resolve nanometer or smaller dimension  
 objects. The real challenge is to achieve an image resolution  
 of 1 nm or smaller by using an energy whose wavelength  
 is much bigger than the object to be imaged without uti-  
 lizing an electron microscope. Here, a stratagem has been  
 formulated to achieve sub-nanometer image resolution, that  
 both overcomes the ADL and also offers an ability of a very  
 high zooming factor for imaging objects from macro dimen-  
 sions down to sub-nanometer dimensions. The main steps are  
 described below.

For the multispectral reconstructive imaging, the wave-  
 length (diffraction) effect is avoided by scanning an object  
 and utilizing the reflected intensity matrix for image generation  
 (see Fig. 1). The reconstructive imaging can be implemented,  
 in principle, by any light source and detector system, simi-  
 lar to what is done in regular topography and tomography,  
 but to be able to see under the surface in a non-destructive  
 fashion, only terahertz is suitable via the RI mode because  
 of its ultra-sensitivity [10]. In this case, a simple tomogram  
 is not enough, as was shown elsewhere [11]. However, here  
 we exploit the Beer-Lambert law, rewritten in terms of the  
 measured reflectance as,  $R = \alpha l \epsilon$ , where  $\alpha$  is the molar absorp-  
 tivity,  $l$  is the path length, and  $\epsilon$  is the dielectric constant.  
 Measured reflectance,  $R$  is a material dependent parameter,  
 thus, also dependent on the position of the incident beam  
 on the sample under measurement, because, the sample (e.g.,  
 a semiconductor wafer) is made of different materials arranged  
 in different patterns. Thus, a 3D matrix of the position depen-  
 dent reflectance is adequate for reconstructing an image of the  
 volume via the algorithm outlined above.

With the advent of this nanoscanner, the resolution limit is  
 partly defined by the smallest step of the positioning system.  
 This is  $\sim 24$  nm for the current setup. Thus, using the algo-  
 rithm as described above, the resolution is enhanced down to  
 less than 1 nm. The algorithm outlined here will only inter-  
 polate the measured data, it never extrapolates; thus, ensures  
 that the results are within the boundaries of the object under  
 investigation. With the combination of an even finer position-  
 ing stage and the algorithm, it is projected that the resolution  
 may be enhanced down to a few Angstroms ( $\text{\AA}$ ).

## III. EXPERIMENTAL

The experimental arrangement was reported elsewhere [10]  
 and reproduced in Fig. 3. An Applied Research & Photonics  
 terahertz nanoscanning spectrometer (TNS) was used for  
 the present investigation. There are two main parts of the  
 TNS, the terahertz module and the nanoscanner module. The  
 terahertz module generates multispectral continuous-wave ter-  
 ahertz energy via the dendrimer dipole (DDE) mechanism [9]

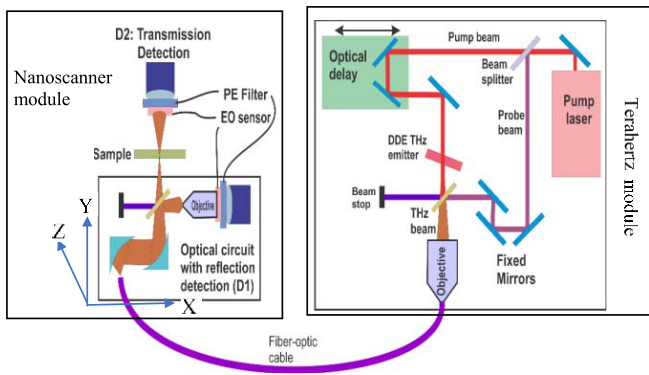


Fig. 3. The optical circuit is mounted on a XYZ nanoscanner (not shown). Both reflection mode and transmission mode measurements are possible. Here, the sample remains stationary while the nanoscanner will scan the sample over a chosen area or volume. Adapted from [10].

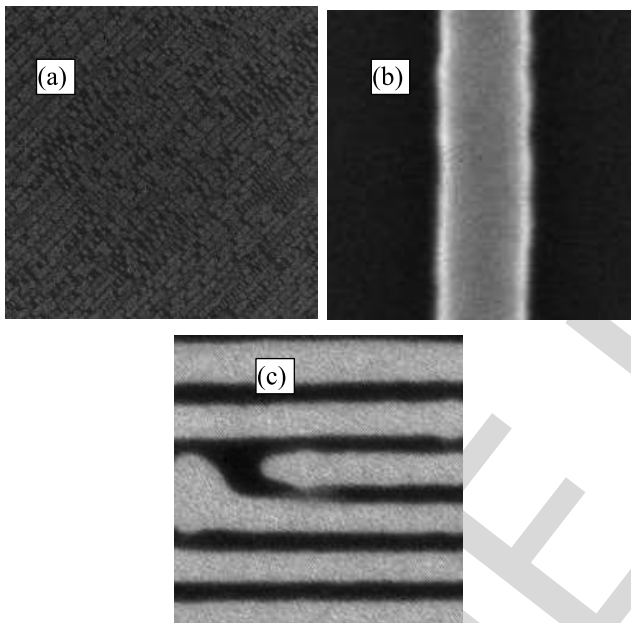


Fig. 4. Comparison with SEM images (from NGR Inc.) of (a)  $70\ \mu\text{m} \times 70\ \mu\text{m}$  area; (b) 70 nm line; and (c) 14 nm lines [8]. Although no scales are shown on the SEM images, the dimensions of each feature are clearly noted in the NGR Inc.'s source file.

268 and also generates time-domain interferogram via an optical  
 269 delay-line. The terahertz beam is coupled to a multimode  
 270 fiber [3] that delivers the beam to the optical circuit located on  
 271 the nanoscanner module. Additionally, the nanoscanner mod-  
 272 ule houses the three orthogonal axes and an optical circuit  
 273 for focusing the terahertz beam on the sample as well as the  
 274 detection system. Both reflection mode and transmission mode  
 275 measurements are possible. Here, the sample remains station-  
 276 ary while the nanoscanner will scan the sample over a chosen  
 277 area or volume. As pointed out before, the nanoscanner has  
 278 a hardware pitch of  $\sim 24\ \text{nm}$  in all three orthogonal directions.  
 279 This is the scanning resolution used for the current measure-  
 280 ments. The scanned data matrix was stored in a data file and  
 281 processed by the aforementioned algorithm as implemented by  
 282 a commercially available software.

TABLE I  
UNITS FOR MAGNETIC PROPERTIES

Feature	NGR Inc. SEM data [8]	Terahertz data
70 nm line pattern	70 nm	$70\ \text{nm} \pm x\ \text{nm}$
14 nm line pattern	14 nm	$\sim 15\ \text{nm} \pm x\ \text{nm}$

$x$  is the standard deviation that could be computed from multiple measurements.

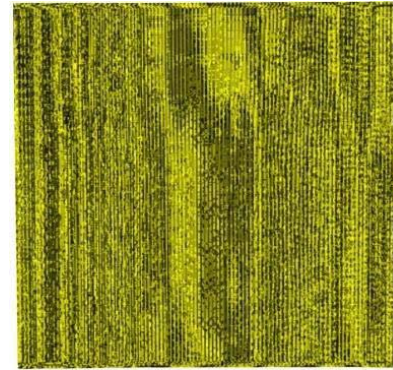


Fig. 5. Terahertz image of a  $100\ \mu\text{m}^2$  area of a test chip with line pattern. This image reveals similar pattern as observed from SEM, Fig. 4(a).

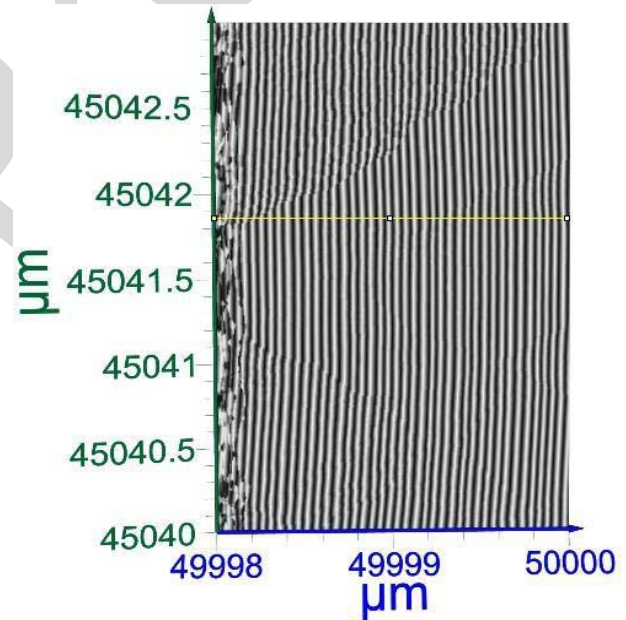


Fig. 6. Close up of line pattern extracted from Fig. 5 over  $2\ \mu\text{m} \times 3\ \mu\text{m}$ . The wiggly lines indicate the grain boundaries.

Two sample chips with different metal line patterns were  
 283 obtained from NGR Inc. [8]. These chips have different types  
 284 of metal lines on them with different dimensions; all deposited  
 285 on the surface of a silicon wafer. As determined by NGR  
 286 Inc. via SEM, the first group of lines are 14 nm wide and  
 287 the second group of lines are 70 nm wide. These data are  
 288 shown in Fig. 4 as supplied by NGR Inc. The as received  
 289 chips were mounted on the TNS one at a time and scanned  
 290 over a small volume. Built-in front end software interface was  
 291 used for data acquisition via aforementioned scanning protocol  
 292 over selected areas and volumes of the chip.  
 293

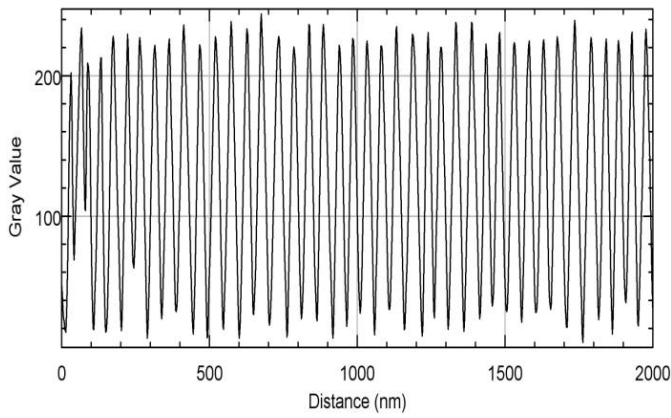


Fig. 7. Graphical analysis of the lines shown in Fig. 6. Individual line's thickness may be quantified. The yellow line in Fig. 6 may be translated at any position over the image for measuring the feature sizes at that location.

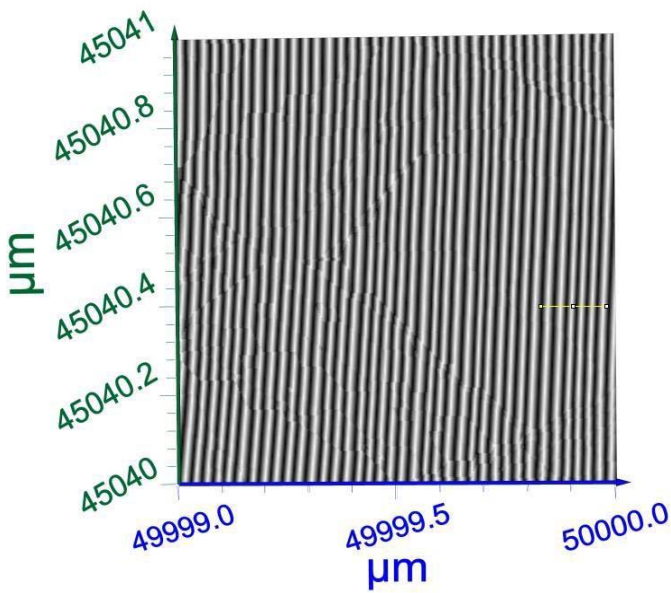


Fig. 8. A closer view of Fig. 6 over  $1 \mu\text{m} \times 1 \mu\text{m}$  shows defects in line pattern.

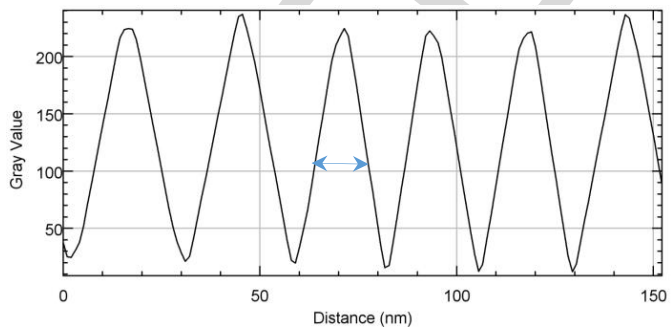


Fig. 9. Graphical analysis of Fig. 8. Calculated line width at the FWHM is  $\sim 15 \pm x$  nm.

IV. RESULTS AND DISCUSSION

Experimental results are compared with the NGR Inc. data as shown in Table I. In Fig. 4 we display three images obtained courtesy of NGR Inc. Fig. 4(a) is a SEM image of

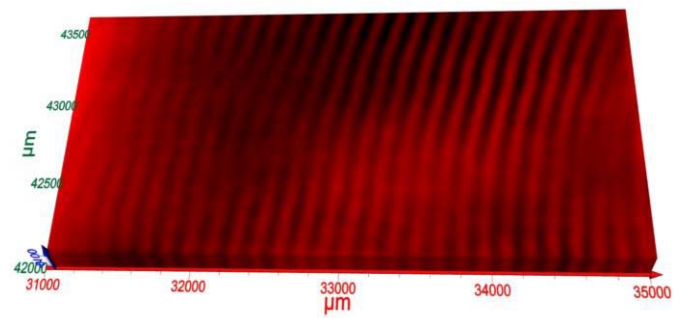


Fig. 10. Terahertz image 3-D rendering of 70 nm lines.

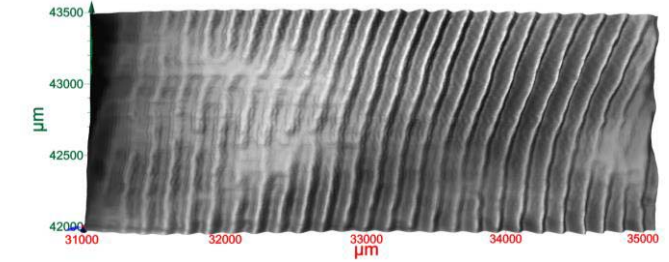


Fig. 11. Defects visible in 70 nm line pattern. Lines are curved presumably due to lack of proper alignment of the sample with respect to the beam.

$70 \mu\text{m}^2$  area of a chip while Fig. 4(b) displays a single metal line of width 70 nm. Fig. 4 (c) shows a line pattern of width 14 nm as reported by NGR Inc.

We now present and analyze the terahertz images. Fig. 5 shows an image of  $100 \mu\text{m}^2$  area of a chip produced by terahertz multispectral reconstructive imaging. Subsequent analysis is presented for 15 nm line patterns and then 70 nm patterns, respectively.

Fig. 6 shows a close-up of the line patterns over  $2 \mu\text{m} \times 3 \mu\text{m}$  area. A graphical analysis across the cursor (yellow line in Fig. 6) is shown in Fig. 7 where a grey scale value was assigned for white = 0 and black = 256. This graph may be used to quantify the line widths by calculating the full width at half maximum (FWHM) of a given line. As shown in Fig. 8, a closer view of Fig. 6 is displayed over  $1 \mu\text{m} \times 1 \mu\text{m}$  area is displayed, while Fig. 9 exhibits a graphical analysis of a few lines in Fig. 8 along the cursor (yellow line). The line width at the FWHM was found to be  $15 \text{ nm} \pm x$ , where  $x$  is the standard deviation that could be quantified by reading the widths of multiple lines from Fig. 8, or equivalently, from Fig. 6 for a higher number of lines.

Fig. 10 displays a 3D view of a segment of the second sample with 70 nm line pattern and a grey-scale surface image of the same is shown in Fig. 11. Many defects are visible. A close-up of Fig. 11 is shown in Fig. 12, and Fig. 13 shows a graphical analysis of the same. The line width at FWHM was found to be  $70 \text{ nm} \pm x \text{ nm}$ , where  $x$  is the standard deviation that could be quantified by reading the widths of multiple lines from Fig. 11 or Fig. 12.

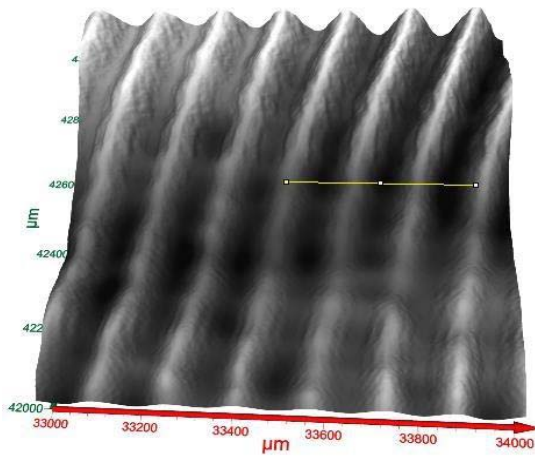


Fig. 12. Close up surface image of a few lines extracted from Fig. 11.

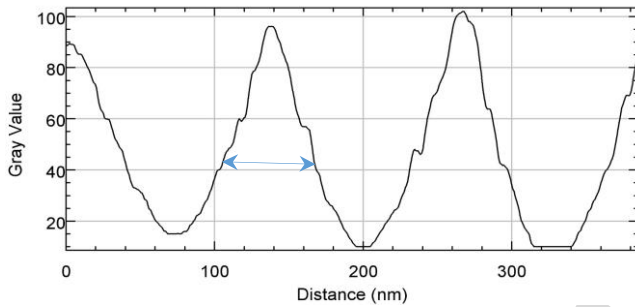


Fig. 13. Graphical analysis of Fig. 12 along the cursor. The patterned lines are  $\sim (70 \pm x)$  nm.

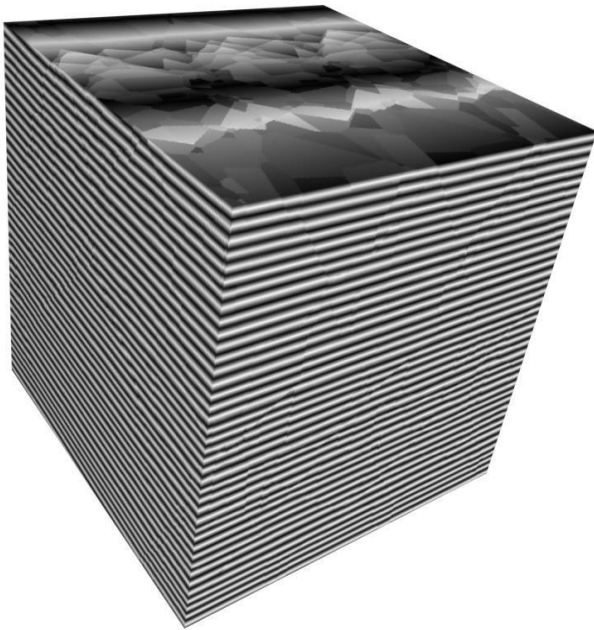


Fig. 14. 3D view of metal lines and their grain structure. 3D view of metal lines and spacings on a chip. Total volume is  $1 \mu\text{m}^3$ .

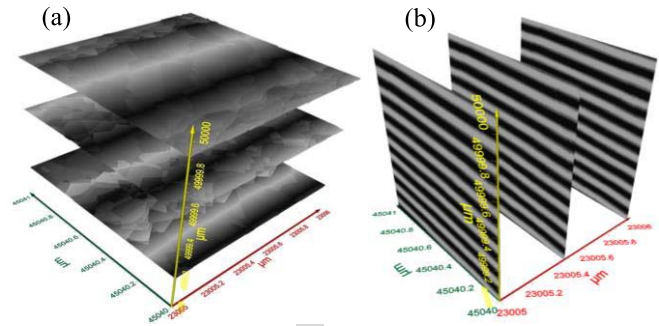


Fig. 15. (a) Layer by layer view of the grain-structure across the depth of the metal lines on the XY plane. (b) Three layers on the YZ plane.

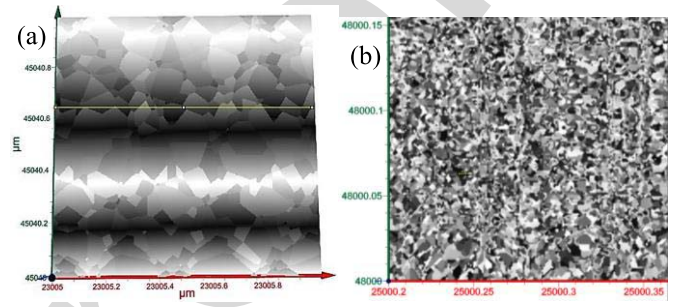


Fig. 16. (a) A single layer's ( $1 \mu\text{m} \times 1 \mu\text{m}$ ) grain structure on metal lines. (b) Surface image of a graphene sample (not discussed here) is used only for the demonstration of  $< 1$  nm resolution (see below).

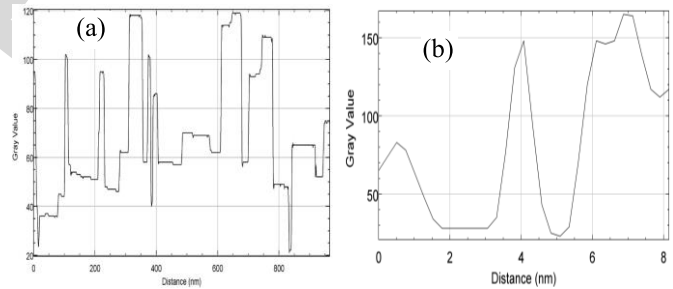


Fig. 17. (a) Analysis of grain sizes along the yellow line of the image above. The yellow line in Fig. 16 (a) may be translated at any position over the image for measuring the feature sizes at that location. (b) The FWHM is  $\sim 0.77$  nm (from Fig. 16 (b)).

on the XY plane have been extracted (Fig. 15(a)). As can be 330  
 seen, the grain pattern is different on different layers. A single 331  
 layer from Fig. 15(a) is shown in Fig. 16(a) whose graphical 332  
 analysis is shown in Fig. 17(a) along the cursor (yellow line in 333  
 Fig. 16(a)). Grain sizes may be quantified, and the size distri- 334  
 bution may also be computed from Fig. 17(a). Other layers on 335  
 the XY plane may be analyzed in a similar fashion. In addition, 336  
 layers may be extracted and analyzed on other orthogonal 337  
 planes, XZ or YZ (Fig. 15(b)). Fig. 16(b) shows a surface 338  
 image of a graphene sample (not discussed in this paper) 339  
 used only to demonstrate sub-nanometer resolution capability. 340  
 Fig. 17(b) displays a graphical analysis of a small feature from 341  
 Fig. 16(b) whose size was determined to be  $\sim 0.77$  nm; thus, 342  
 demonstrating sub-nanometer resolution. 343

### 327 A. Layer by Layer Inspection and Grain-Image

328 Fig. 14 shows a 3D view of  $1 \mu\text{m}^3$  volume of the first 329  
 chip containing 14 nm lines from which 3 different layers

## V. CONCLUSION

We have demonstrated terahertz multispectral reconstructive imaging of nanometer sized metal lines fabricated on a silicon wafer; thereby demonstrating that the Abbe diffraction limit has been overcome for higher resolution imaging. It was further demonstrated that while overcoming the Abbe diffraction limit is a required condition, it is not sufficient for achieving sub-nanometer resolution. A stratagem was implemented via a nanoscanner, and reflectance measurements were conducted by exploiting the Beer-Lambert law written in terms of the reflectance. A continuous wave terahertz system was used in conjunction with the said 3D nanoscanner for scanning a small volume of the samples under investigation. The “inverse distance to power equations” was used for both 2D and 3D image formation and analysis. The terahertz images were further analyzed by a graphical technique for computing the line widths from the FWHM. It was found that the line widths obtained from terahertz images are in good agreement with the corresponding SEM images. Additionally, layer by layer analysis was demonstrated by dividing the terahertz images into a number of slices. Grains are clearly visible on the metal lines; their sizes may be quantified by the same graphical means as used for the line widths. Unlike electron microscope techniques where the samples must be cut to fit in the vacuum chamber and must be thin enough for electron beam transparency, terahertz imaging is a non-destructive, non-contact technique without any laborious sample preparation. There are no restrictions on the sample size or shape. The technique described herein, therefore, may be used for analysis of semiconductor features in a non-destructive, non-contact mode during the process development and at the post-process stages after device fabrication. The system can be used either in a laboratory setting or in a cleanroom environment. In addition, nanoparticles’ size and size distribution may also be measured by this technique.

## ACKNOWLEDGMENT

Anis Rahman wishes to acknowledge help from Mr. Michael Hoffman of Designlynx Technology for obtaining the samples from NGR Inc.

## REFERENCES

- [1] E. Abbe, “Beiträge zur theorie des mikroskops und der mikroskopischen wahrnehmung,” *Archiv Für Mikroskopische Anatomie*, vol. 9, no. 1, pp. 413–418, 1873.
- [2] L. Novotny and B. Hecht, “Propagation and focusing of optical fields,” in *Principles of Nano-Optics*. Cambridge, U.K.: Cambridge Univ. Press, 2006, pp. 45–87.
- [3] A. Rahman, A. K. Rahman, T. Yamamoto, and H. Kitagawa, “Terahertz sub-nanometer sub-surface imaging of 2D materials,” *J. Biosens. Bioelectron.*, vol. 7, no. 3, pp. 1–8, 2016, doi: [10.4172/2155-6210.1000221](https://doi.org/10.4172/2155-6210.1000221).
- [4] A. Rahman and A. K. Rahman, “Terahertz spectroscopic analysis and multispectral imaging of epitaxially grown semiconductors with nanometer resolution,” *J. Biosens. Bioelectron.*, vol. 7, no. 4, pp. 1–6, 2016, doi: [10.4172/2155-6210.1000229](https://doi.org/10.4172/2155-6210.1000229).

- [5] A. Rahman, A. K. Rahman, and B. Rao, “Early detection of skin cancer via terahertz spectral profiling and 3-D imaging,” *Biosens. Bioelectron.*, vol. 82, pp. 64–70, Aug. 2016.
- [6] J. C. Davis, *Statistics and Data Analysis in Geology*. New York, NY, USA: Wiley, 1986, pp. 238–244.
- [7] R. Franke, “Scattered data interpolation: Tests of some methods,” *Math. Comput.*, vol. 33, no. 157, pp. 181–200, 1982.
- [8] M. Hoffman, private communication, Oct. 2016.
- [9] A. A. Rahman, A. Rahman, and D. A. Tomalia, “Dendrimer dipole excitation: A new mechanism for terahertz generation,” *J. Biosens. Bioelectron.*, vol. 7, no. 1, pp. 1–6, 2016, doi: [10.4172/2155-6210.1000196](https://doi.org/10.4172/2155-6210.1000196).
- [10] A. Rahman, A. K. Rahman, and D. A. Tomalia, “Engineering dendrimers to produce dendrimer dipole excitation based terahertz radiation sources suitable for spectrometry, molecular and biomedical imaging,” *Nanoscale Horizons*, vol. 2, no. 20, pp. 127–134, Mar. 2017, doi: [10.1039/c7nh00010c](https://doi.org/10.1039/c7nh00010c).
- [11] A. Rahman, “Terahertz multispectral imaging of epitaxially grown semiconductors’ lattice defects,” in *Proc. ASMC*, 2017, pp. 45–50.



**Anis Rahman** was born in Pabna, Bangladesh. He received the B.Sc. (Hons.) and M.Sc. degrees (First Class) in physics from the University of Rajshahi, Bangladesh, the M.S. degree and the Ph.D. degree in electrical and computer engineering in 1994 with Marquette University. From 1981 to 1985, he was a Scientific Officer of Bangladesh Atomic Energy Commission. He was a Post-Doctoral Researcher with Columbia University under Prof. N. Turro and Prof. C. Durning.

He is an acclaimed Scientist in the field of nanotechnology. He was a recipient of many scientific awards, including NASA Nanotech Brief’s “Nano-50” Award twice, the CLEO/Laser Focus World’s “Innovation Award,” and the “2015 MP Corrosion Innovation of the Year,” by the NACE.

Dr. Rahman is the Founder of Applied Research and Photonics a leading terahertz company located in Harrisburg, PA, USA. His invention of “Dendrimer Dipole Excitation,” a new mechanism for terahertz generation, makes it possible to generate high power terahertz radiation. He was also a recipient of many awards from other scientific organizations such as the OMICS International Keynote Recognition and Center for Dermal Research of Rutgers University, the Center for Entrepreneurial Leadership Award by the Juniata College of Pennsylvania, and community awards. He is a recognized Scientific Leader and a member of professional organizations, including the American Chemical Society (ACS) and SPIE, and a Senior Member with Optical Society of America. In 2017, he was elected the Chair of OSA’s metrology technical group. He is the Past Chair of the Small Chemical Businesses Division of the ACS.



**Aunik K. Rahman** was born in Dhaka, Bangladesh. He received the B.S. degree in electrical engineering from Rensselaer Polytechnic Institute, Troy, NY, USA, in 2006. Since then he has been with Applied Research and Photonics (ARP) as an Engineer.

His research experience includes design and implementation of terahertz instruments for reconstructive imaging and time-domain spectroscopy. He was a recipient of many achievement awards for his research at ARP.